Physica E 174 (2025) 116333

Contents lists available at ScienceDirect

Physica E: Low-dimensional Systems and Nanostructures

journal homepage: www.elsevier.com/locate/physe

Effect of electric field on excitons in wide quantum wells

Shiming Zheng, E.S. Khramtsov *, I.V. Ignatiev

Spin Optics Laboratory, St. Petersburg State University, Ulyanovskaya 1, Peterhof, St. Petersburg, 198504, Russia

ARTICLE INFO

Editor: Ming-Wei Wu

Keywords:
Exciton
Quantum wells
Electric field
Stark shift
Exciton-light coupling
Dipole moment

ABSTRACT

A microscopic model of a heterostructure with a quantum well (QW) is proposed to study exciton properties in an external electric field. The effect of an electric field ranging from 0 to 6 kV/cm applied to a GaAs/AlGaAs QW structure in the growth direction is studied for several QWs of various widths up to 100 nm. The three-dimensional Schrödinger equation (SE) for the exciton is numerically solved using the finite difference method. Wave functions and energies of several states of the heavy-hole and light-hole excitons are calculated. The dependencies of exciton state energy, binding energy, radiative broadening, and static dipole moment on the applied electric field are determined. Additionally, the threshold for exciton dissociation in the 100-nm QW is established. Furthermore, we calculate an electric-field-induced shift in the center of mass of heavy-hole and light-hole excitons in the QWs. Finally, we simulate the reflection spectra of heterostructures with GaAs/AlGaAs QWs under an electric field using the calculated energies, radiative broadenings, and phases of exciton resonances.

1. Introduction

Quantum well (QW) spectroscopy allows one to study both the exciton states of motion as a whole and the effects of quantum confinement on the relative motion of an electron and a hole in an exciton [1–3]. The quantized states of the exciton center-of-mass motion are studied in wide QWs, whose thickness exceeds the exciton Bohr radius, a_B, by an order of magnitude [4,5]. The quantization of the exciton motion results in the appearance of discrete energy levels, which manifest themselves as resonances in reflection and photoluminescence spectra [5–12]. In narrow QWs, whose widths are comparable to a_B, the spatial constraint affects the relative motion of the electron and the hole in the exciton. This leads to an increase in the exciton energy and its binding energy, as it is reported in many publications see, e.g., [13–21].

External fields applied to heterostructures with QWs enable the observations of various physical phenomena related to the influence of these fields on quantized exciton states. The application of an electric field to semiconductor heterostructures is perhaps the most important research area, both from a practical point of view and for studying new effects, see, e.g., Refs. [22–25]. Recent studies have also explored the impact of electric fields on excitonic states in cuprous oxide, revealing fine structure splittings and Stark ladder formations [26–28]. Most studies of this kind have been performed for narrow QWs [29–38]. In these and many other works, it has been demonstrated that the electric field can strongly modify the relative motion of an electron and a hole in an exciton. This leads to the Stark effect, which manifests itself as a change in the exciton energy. In addition, the electric field reduces the exciton-light interaction, which is observed as significant changes in the optical spectra of excitons. These effects become noticeable in narrow QWs when a sufficiently strong electric field on the order of tens of kV/cm is applied.

In double QWs, the electric field controls the lifetime of an exciton, enables switching the exciton type from direct to indirect, and modifies both the binding energy and the exciton oscillator strength [39–43]. In wide QWs, the electric field induces the inversion of spectral oscillations in the reflection spectra [44].

Applying a constant electric field with a controllable magnitude in practical works can be a challenging problem. Specifically, the presence of free charge carriers in real heterostructures can lead to their redistribution under the applied voltage, partially screening the electric field. This circumstance significantly complicates the interpretation of the results of experiments in electric fields compared, for example, with experiments in magnetic fields, where there is no movement of charge carriers induced by the field. In this regard, experimental conditions in magnetic fields are more controllable, and many papers have been devoted to excitons in magnetic fields, see, e.g., Refs. [45–50].

Excitons in QWs of intermediate widths, from $L_{QW} \approx 2a_B$ to $L_{QW} \approx 10a_B$, have been relatively understudied in electric fields [23]. In a recent work [24], the authors experimentally studied excitons in a single GaAs/AlGaAs QW with a width of $L = 30$ nm under external electric fields of up to 5 kV/cm using reflectance spectroscopy. The

* Corresponding author.
E-mail address: e.khramtsov@spbu.ru (E.S. Khramtsov).

https://doi.org/10.1016/j.physe.2025.116333
Received 26 March 2025; Received in revised form 10 July 2025; Accepted 18 July 2025
Available online 30 July 2025

authors had to use additional optical excitation of the sample to achieve an electric field of controllable strength. Excitons in the QW were used as sensors for the electric field magnitude. To determine the exact value of the applied electric field, the authors compared the experimental reflectance spectra of the heterostructure under study with theoretical calculations. Several exciton states were investigated, and a consistent field strength was obtained.

The goal of this paper is to extend the theoretical results obtained in Ref. [24], specifically to conduct an in-depth theoretical study of the dependence of exciton energy, exciton-light coupling, and exciton dipole moment in relatively wide QWs on the applied electric field. These exciton characteristics are studied for several states, which can be observed experimentally [24]. In narrow QWs studied earlier [29–31,34,40], a relatively weak electric field on the order of several kV/cm is sufficient to induce a change in the potential energy of a charge carrier comparable to the exciton binding energy, E_b, at a distance of approximately the exciton Bohr radius. For example, an electric field of $F = 6$ kV/cm results in an energy change of $\Delta E = 4.3$ meV at $a_B \approx 15$ nm, which is the Bohr radius of an exciton in GaAs. This energy change is close to E_b in bulk GaAs. Thus, QWs with a width $L > 2a_B \approx 30$ nm can be considered intermediate in width, lying between narrow and wide QWs [1].

A rectangular GaAs/$Al_{0.3}Ga_{0.7}As$ QW with a finite potential well depth is considered. The heterostructure under study contains a single QW with widths of 30, 50, or 100 nm. The QW with an intermediate width of $L = 30$ nm is considered because the effects of the electric field in this QW can be described by perturbation theory. In wider QWs, $L = 50$ nm and 100 nm, exciton properties exhibit strongly nonlinear behavior. Thus, this study allows us to trace the transition from a relatively narrow QW to wide QWs.

Microscopic modeling was performed to analyze exciton states under electric fields ranging from 0 to 6 kV/cm. The electric field is assumed to be applied in the direction of the heterostructure growth. We consider several exciton states, which can be experimentally identified and studied in QWs of this width. In wider QWs, exciton resonances may overlap [12], making the interpretation of results more challenging.

The exciton states in the QWs were described by numerically solving the three-dimensional Schrödinger equation (SE) using the fourth-order finite difference method (FDM). The energies and wave functions of the exciton states were obtained for various electric field strengths. The wave functions were then used to calculate the radiative broadening, the static dipole moments, and the center-of-mass displacement of the exciton based on well-known formulas [1]. Finally, we model reflectance spectra of heterostructures with the QWs in electric fields, which can be observed experimentally.

2. Basic theory

A single electron can be described in the Cartesian coordinate system by three spatial coordinates (x, y, and z). Hereafter it is assumed that the x and y coordinates lie within the QW layer, why the z coordinate is directed along the growth axis of the heterostructure. The effective mass of an electron is assumed to be isotropic in all three directions and is equal to m_e. The hole states are described by the Luttinger Hamiltonian [51], due to the degeneration of the valence band in GaAs-type crystals. Consequently, the effective mass of the hole becomes anisotropic and can be expressed in terms of the Luttinger parameters. Namely, the effective mass of a hole along the z axis, m_{hz}, is not equal to the effective mass of a hole in the xy plane, m_{hxy}. At the same time, it is assumed to be isotropic in the QW plane, $m_{hx} = m_{hy} \equiv m_{hxy}$.

We consider QWs of finite width, where the heavy-hole and light-hole states are split by the quantum confinement effect. In this case, we can neglect the heavy-hole-light-hole mixing effects and consider Xhh and Xlh excitons separately. The analysis carried out in a number of works [16,21,52,53] shows that the mixing effects are insignificant compared to the electric-field-induced effects discussed in this paper. Therefore, we consider here only the diagonal part of the Luttinger Hamiltonian [54]. We also do not account for spin interactions within the exciton, as they are negligible when the magnetic field is not considered [1]. We consider the excitons at zero temperature, i.e., we do not take into account any temperature-induced effects. A quantitative analysis of thermal effects lies beyond the scope of the present work and would require a separate, dedicated study.

The time-independent six-dimensional SE can be used to describe the quantum mechanical behavior of each type of exciton, taking into account the Coulomb interaction between the hole and the electron. The SE for an exciton is given by:

$$\left[\hat{K}(x_h, y_h, z_h, x_e, y_e, z_e) - \frac{q^2}{\varepsilon \cdot r} + V_e(z_e) + V_h(z_h)\right] \psi(x_h, y_h, z_h, x_e, y_e, z_e) = E \cdot \psi(x_h, y_h, z_h, x_e, y_e, z_e). \quad (1)$$

Here, $\hat{K}$ is the exciton kinetic energy operator, ε is the dielectric constant, r is the distance between the electron and the hole, q is the absolute value of the electron charge, V_e and V_h are the potential barriers for the electron and the hole, respectively; z_e and z_h are the z coordinates for the electron and the hole, respectively. The SE (1) allows one to find the exciton wave function ψ and the exciton energy E.

The operator $\hat{K}$ can be expressed as follows:

$$\hat{K} = -\frac{\hbar^2}{2m_e}\nabla_e^2 - \frac{\hbar^2}{2m_{hxy}}\nabla_h^2 - \frac{\hbar^2}{2m_e}\frac{\partial^2}{\partial z_e^2} - \frac{\hbar^2}{2m_{hz}}\frac{\partial^2}{\partial z_h^2}. \quad (2)$$

Here ∇^2 is the Laplace operator in the xy plane.

The electric field is assumed to be applied along the z axis, coinciding with the growth axis of the heterostructure. In the presence of an electric field, the QW potential profile for both the electron and the hole changes from a rectangular shape to a trapezoidal one. Therefore, we can express the potential energy of the electron and the hole as follows:

$$V_e = -qFz_e + \begin{cases} 0, & \text{if } |z_e| < L/2 \\ V_{e0}, & \text{if } |z_e| \geq L/2 \end{cases} \quad (3)$$

$$V_h = qFz_h + \begin{cases} 0, & \text{if } |z_h| < L/2 \\ V_{h0}, & \text{if } |z_h| \geq L/2 \end{cases} \quad (4)$$

Here F is the electric field strength, and V_{e0} and V_{h0} are, respectively, the potential energies of the electron and the hole outside the QW.

The exciton can freely move along the QW layer. Accordingly, we can introduce the coordinates of the center-of-mass motion in the xy plane:

$$X = \frac{m_{hxy} \cdot x_h + m_e \cdot x_e}{m_{hxy} + m_e}; Y = \frac{m_{hxy} \cdot y_h + m_e \cdot y_e}{m_{hxy} + m_e}. \quad (5)$$

Using these variables, the exciton wave function can be factorized:

$$\psi(x_h, y_h, z_h, x_e, y_e, z_e) = \psi(z_e, z_h, \rho, \theta) e^{iK_X X} e^{iK_Y Y}, \quad (6)$$

where $e^{iK_X X}$ and $e^{iK_Y Y}$ are the plane waves describing the exciton motion. The wave function $\psi(z_e, z_h, \rho, \theta)$ describes the relative motion of the electron and the hole in the exciton, as well as their motion across the QW layer.

In Eq. (6), we used the cylindrical system of coordinates, in which the relative electron–hole motion in the xy plane is described by coordinates ρ and θ. Here θ is the angle between the vector $\vec{\rho}$ and the coordinate x in the plane, and $|\vec{\rho}|$ is described by expression,

$$\rho \equiv |\vec{\rho}| = \sqrt{(x_e - x_h)^2 + (y_e - y_h)^2}. \quad (7)$$

In what follows, we use the cylindrical symmetry of the exciton problem. In this case, we can further factorize the exciton wave function:

$$\psi(z_e, z_h, \rho, \theta) = \psi(z_e, z_h, \rho) e^{ik_\theta \theta}, \quad (8)$$

where $k_\theta = 0, 1, 2, \ldots$ is the orbital quantum number describing the angular dependence of the exciton wave function [5,54].

The factorizations (6) and (8) allow us to simplify the SE for the exciton in a QW to a three-dimensional form [5]:

$$\left(-\frac{\hbar^2}{2\mu_{xy}}\left[\frac{\partial^2}{\partial\rho^2}-\frac{1}{\rho}\cdot\frac{\partial}{\partial\rho}+(1-k_\theta{}^2)\cdot\frac{1}{\rho^2}\right]-\right.$$
$$\left.\frac{\hbar^2}{2m_e}\frac{\partial^2}{\partial z_e^2}-\frac{\hbar^2}{2m_{hz}}\frac{\partial^2}{\partial z_h^2}-\frac{q^2}{\varepsilon\cdot r}+V_e+V_h\right)\chi(\rho,z_e,z_h) \tag{9}$$
$$=E_X\cdot\chi(\rho,z_e,z_h).$$

Here E_X is the exciton energy with respect to the bandgap energy E_g and $\mu_{xy} = m_e m_{hxy}/(m_e + m_{hxy})$ is the reduced effective mass of the exciton in the plane. In Eq. (9) we used the substitution, $\chi(z_e, z_h, \rho) = \psi(z_e, z_h, \rho)\cdot\rho$, to avoid divergence at the coinciding coordinates of the electron and the hole [5,21,54–56]. In what follows, we consider only the case of $k_\theta = 0$, since only such exciton states interact with light [1].

3. Calculations of exciton characteristics in electric fields

3.1. Exciton energy

The energy of an exciton is most often calculated using the variational method to solve the SE [16,57,58]. However, this method allows for the calculation of the exciton ground state predominantly. The calculations of excited states meet certain problems [41–43]. The accuracy of the calculated wave functions depends on the trial functions, which have to be chosen manually. Therefore, the accuracy is unknown a priori.

Recently, numerical methods for solving the SE have been extensively used, which do not require the trial functions [5,19,21,24,48,59]. One such method is based on the finite difference method (FDM). The central idea of the FDM is to represent the Hamiltonian of SE (9) as a matrix on a grid. The method can provide accurate numerical results when the grid step is sufficiently small. Another approach involves expanding the wave function in a basis of B-splines [27], which allows one to solve a similar problem. To obtain the exciton state energies and wave functions, we must calculate the eigenvalues and eigenvectors of the matrix. In fact, only a few of the lowest exciton states that are observed in the experiment are of interest. These states can be efficiently computed using the well-known Arnoldi algorithm [5,60].

The exponential decay of function χ at large values of variables allows us to impose zero boundary conditions at the boundary of a three-dimensional domain. The domain slightly exceeds the width of the QW layer to account for the tails of the exciton wave functions due to their penetration into the barrier layers. For the 30-nm and 50-nm QWs, we have chosen the domain size to be ≈ 65 nm along the z_e and z_h coordinates, and approximately 130 nm along the ρ coordinate. For the 100 nm QW, the domain size along the z_e and z_h coordinates has been chosen to be twice as large. We take into account the difference in the mass of the charged carriers in the QW and the barrier layers. However, the Bastard boundary condition [61], which ensures continuity of the carrier flux across the heterointerface, is not applied in our calculations for the sake of simplicity. Theoretical analysis [62,63] indicates that this condition has only a minor effect on the exciton energy in wide QWs, a few percent for the 30-nm QW and even less for the 50-nm and 100-nm QWs considered in this work. We also neglect the small discontinuity in the dielectric constants of the QW and the barrier layers, as its effect is negligible for the relatively wide QWs under study [62,64,65]. The calculation step ranges from 1 nm to ≈ 0.4 nm. It has been verified that the smallest spatial step used in the numerical calculations is sufficient to accurately model the Coulomb potential. Accordingly, extrapolation of the numerical results to zero step yields all exciton characteristics with an accuracy of approximately 0.1% or better. Further details of the numerical calculations can be found in Refs. [5,19,21,48].

3.2. Exciton binding energy

The obtained exciton energies can also be used to determine the exciton binding energies. To this end, the energies of the quantum-confined electron (E_e) and hole (E_h) states should be calculated. The respective SE for a free electron in a QW takes the form of a one-dimensional equation [66]:

$$\left(-\frac{\hbar^2}{2m_e}\frac{\partial^2}{\partial z_e^2}+V_e\right)\psi(z_e)=E_e\cdot\psi(z_e). \tag{10}$$

Due to the exponential decay of the wave function $\psi(z_e)$ at a significant distance from the QW, zero boundary conditions are imposed, ensuring that the wave function vanishes at the edges of the considered region. The solution of Eq. (10) is straightforward and can be obtained with high accuracy [66]. The solution of Eq. (10) yields the energies of the quantum-confined electron states i, E_{ei}. Each such energy represents a lower boundary of a minizone corresponding to a free propagation of the electron along the QW layer with kinetic energy, $E_{e,kin} = \hbar^2 k_e^2/(2m_e^*)$ [19]. A similar equation can be written for a free hole in the QW by replacing the index $e \to h$. The hole energies, E_{hi}, and respective minizones can be obtained from such equation.

The exciton energy can be expressed as the sum of the free electron and free hole energies minus their binding energy:

$$E_X = E_e + E_h - E_b. \tag{11}$$

This equation allows one to calculate the binding energies for the lowest heavy-hole and light-hole exciton states using solutions of Eqs. (9) and (10). However, for higher-energy exciton states, the calculations may encounter difficulties when the states fall into the minizone band. In such cases, more advanced computational techniques, such as the complex-coordinate rotation method or the stabilization method, should be employed [26,56]. Consequently, the binding energy in this case is effectively zero.

3.3. Exciton-light coupling

The interaction of an exciton with light can be characterized by a constant Γ_0, which represents the radiative decay rate of the electromagnetic wave emitted by the exciton. In experiments, the radiative broadening, $\hbar\Gamma_0$, of exciton resonances can be measured in reflection spectra [21,24,59]. Therefore, theoretical modeling of this broadening and its dependence on the applied electric field is of particular interest [41–43,67].

The exciton wave function obtained by solving the SE (9) enables the calculation of $\hbar\Gamma_0$ within the framework of the non-local dielectric response theory [1].

$$\hbar\Gamma_0 = \frac{2\pi k}{\varepsilon}\left(\frac{e|p_{cv}|}{m_0\omega_0}\right)^2\left|\int_{-\infty}^{\infty}\Phi(z)e^{ikz}dz\right|^2. \tag{12}$$

Here, k represents the wave vector of the light wave, ω_0 denotes the exciton resonance frequency, and $|p_{cv}| = m_0\cdot E_p/2$ is the matrix element of the momentum operator, calculated using the one-electron states of the conduction and valence bands, where $E_p = 28.8$ eV [68]. The function $\Phi(z)$ represents the cross-section of the exciton wave function along the coinciding coordinates of the electron and the hole, defined as $\Phi(z) = \psi(z_e = z_h = z, \rho = 0)$. The integral in Eq. (12) is commonly referred to as the overlap integral of the light wave and the exciton wave function. This integral primarily determines the exciton-light coupling strength.

3.4. Static dipole moment

In an electric field applied to the QW along the growth direction, the exciton becomes polarized. The electron and the hole in the exciton are displaced by the electric field to opposite potential barriers of the

QW, thus creating a static dipole moment for the exciton. The dipole moment of the exciton states can be calculated using the formula,

$$D_X = q \cdot \langle \psi(z_e, z_h, \rho) | (z_e - z_h) | \psi(z_e, z_h, \rho) \rangle. \tag{13}$$

In the cylindrical coordinate system, this formula is transformed to

$$D_X = q \cdot \int |\psi(z_e, z_h, \rho)|^2 (z_e - z_h) \cdot \rho d\rho dz_e dz_h. \tag{14}$$

The dipole moment of an exciton is proportional to the average distance between the electron and the hole. Obviously, the dipole moment is zero in the absence of an electric field for QWs with a symmetric potential. In the presence of an electric field, we can expect that, in the general case, the dipole moment of an exciton in a QW depends nonlinearly on the applied electric field. Indeed, the distance between the electron and hole cannot exceed the QW width. Therefore, the magnitude of the dipole moment should saturate at high field strengths.

3.5. Exciton center-of-mass position

An exciton is a neutral quasiparticle, and its center of mass, at first glance, should be insensitive to an electric field. However, this is not the case. The fact is that the masses of the electron and the hole are different, which causes the exciton to shift towards the heavier particle in an electric field. The calculation of an expectation value of the center-of-mass position is similar to that of the dipole moment,

$$Z = \left\langle \psi(z_e, z_h, \rho) \left| \frac{m_e z_e + m_h z_h}{m_e + m_h} \right| \psi(z_e, z_h, \rho) \right\rangle. \tag{15}$$

As we demonstrate in the next section, the shift can be significant, in particular, for the heavy-hole exciton.

4. Results

We consider in this paper the heterostructure GaAs/$Al_xGa_{1-x}As$ with a parameter x of 0.3, representing the atomic fraction of Al in the barrier $Al_xGa_{1-x}As$. The semiconductor layer GaAs can work as a QW for the electron and the hole because its bandgap energy, $E_g \approx 1.52$ eV [21,68], is smaller than that of the solid solution in the barriers. Moreover, the GaAs layer surrounded by the $Al_xGa_{1-x}As$ barriers creates a potential well both for the electron and the hole, so that this is a type-I heterostructure. In our calculations, we use the sum of potential well depths $V_{e0} + V_{h0} = 365$ meV, and their ratio, $V_{e0}/V_{h0} = 0.65/0.35$, commonly accepted in the literature for the GaAs/$Al_xGa_{1-x}As$ heterostructures [58].

Material parameters used for the calculations of exciton states in the QWs are taken from Ref. [58,68] for GaAs and AlAs and adopted for the barrier layers AlGaAs with 30% concentration of Al. The dielectric constant $\varepsilon = 12.53$ for the GaAs QW and $\varepsilon = 11.8$ for the AlGaAs barriers. The effective mass of the electron is $m_e = 0.067m_0$ in the QW and $0.0919m_0$ in the barriers. For the effective masses of the heavy and light holes, the following equations must be used:

$$\begin{aligned} m_{hhz} &= \frac{m_0}{\gamma_1 - 2\gamma_2}, \; m_{lhz} = \frac{m_0}{\gamma_1 + 2\gamma_2} \\ m_{hhxy} &= \frac{m_0}{\gamma_1 + \gamma_2}, \; m_{lhxy} = \frac{m_0}{\gamma_1 - \gamma_2} \end{aligned} \tag{16}$$

where γ_1 and γ_2 are the Luttinger parameters. For the GaAs, $\gamma_1 = 6.98$ and $\gamma_2 = 2.06$, and for the AlAs, $\gamma_1 = 3.76$ and $\gamma_2 = 0.82$ [68]. Subsequently, the hole masses are: $m_{hhz} = 0.350m_0$, $m_{hhxy} = 0.111m_0$, $m_{lhz} = 0.090m_0$, $m_{lhxy} = 0.203m_0$. The masses of the heavy and light holes for the AlGaAs barriers are obtained by a linear interpolation between the hole masses of GaAs and AlAs: $m_{hhz} = 0.386m_0$, $m_{hhxy} = 0.143m_0$, $m_{lhz} = 0.119m_0$, $m_{lhxy} = 0.244m_0$.

We consider single QWs of three different widths, $L = 30$, 50, and 100 nm. The Bohr radius of the exciton in the GaAs crystal is approximately 15 nm [1]. Therefore, the 30-nm and 50-nm QWs are both of moderate width, but these QW widths provide the excitons with a certain degree of spatial freedom. The 100-nm QW is considerably wider than the exciton Bohr radius, offering more space for exciton polarization in the electric field. Considering these three QWs sizes, we demonstrate how the response of exciton states to the external electric field becomes stronger as the QW width increases.

4.1. Stark shift and binding energy of exciton states in QW

The total energy of the exciton in the QW varies under the influence of an external electric field. Results of microscopic calculations of exciton energies in the studied QWs are shown in Fig. 1. Three exciton states, the first (Xhh1) and second (Xhh2) quantum-confined states of the heavy-hole exciton, and the first quantum-confined state (Xlh1) of the light-hole exciton, can be reliably identified in the calculations. The higher-energy exciton states overlap with a continuous spectrum of motion of free electrons and holes along the QW layer. Their numerical calculation using the approach exploited in this work encounters significant difficulties, as described, e.g., in Refs. [21,56]. The lower boundaries of the continuous spectrum for the pair (free electron + heavy hole, $E_{e1}+E_{hh1}$) are shown in Fig. 1 by the orange dashed curves.

All exciton states experience a Stark shift to the lower-energy region when an electric field is applied. The shift is relatively small for the 30-nm QW (a few meV), moderate for the 50-nm QW, and large for the 100-nm QW (tens of meV). Moreover, for the 30-nm QW, it can be well approximated by a parabolic dependence on the electric field throughout the considered range, $F \leq 6$ kV/cm. In the wider QWs, the parabolic approximation is appropriate only within a smaller field range. In particular, the Stark shift of the Xhh1 and Xlh1 exciton states tends to be approximately linear in an electric fields $F > 1.5$ kV/cm in the 100-nm QW. The boundary of the continuous spectrum ($E_{e1}+E_{hh1}$) also experiences the Stark shift, reducing the energy distance between the Xhh1 state and this boundary. As a result, the Xhh2 state enters into the region of the continuous spectrum and cannot be accurately determined beyond certain electric field values, as indicated in Fig. 1.

When the electric field strength is sufficiently low, the change in the exciton energy, that is the Stark shift, can be analyzed within the framework of perturbation theory [69]. The Stark shift is determined by the potential energy operator $qF(z_e - z_h)$ and is described by the second-order perturbation formula:

$$\begin{aligned} E_{x1} &= E^0_{x1} - \\ &(qF)^2 \cdot \sum_{j \neq 1} \frac{\left| \left\langle \psi(z_e, z_h, \rho)^0_j | (z_e - z_h) | \psi(z_e, z_h, \rho)^0_1 \right\rangle \right|^2}{E^0_{xj} - E^0_{x1}} \\ &\equiv E^0_{x1} - AF^2. \end{aligned} \tag{17}$$

Here E^0_{x1} and E^0_{xj} are the energies of the ground state and the jth excited state of the exciton in the QW without external perturbation. Similarly, $\psi(z_e, z_h, \rho)^0_1$ and $\psi(z_e, z_h, \rho)^0_j$ are respective wave functions in the cylindrical coordinate system in the absence of the electric field. The summation in Eq. (17) is performed over all the excited states. It can be seen from this expression that, under the condition of satisfying the perturbation theory, the Stark energy shift should be a quadratic function of the external electric field strength.

It is instructive to estimate the magnitude of the Stark shift of the Xhh1 state, taking into account only one term of the sum in Eq. (17), namely, the coupling of the Xhh1 and Xhh2 states. The curve calculated in this way for the 30-nm QW is shown in the upper panel of Fig. 1. As seen, this curve shows a slightly smaller Stark shift than that in the exact numerical calculations. The curvature coefficient A [see Eq. (17)] obtained in the perturbation theory is $A = -0.045$ meV/(kV/cm)^2. This value is about 70% of that found from exact numerical calculations ($A_{exact} = -0.064$ meV/(kV/cm)^2). This means that the Xhh1-Xhh2 coupling gives the main contribution to the Stark shift of the Xhh1 exciton state in this QW. In the 50-nm and 100-nm QWs, the perturbation

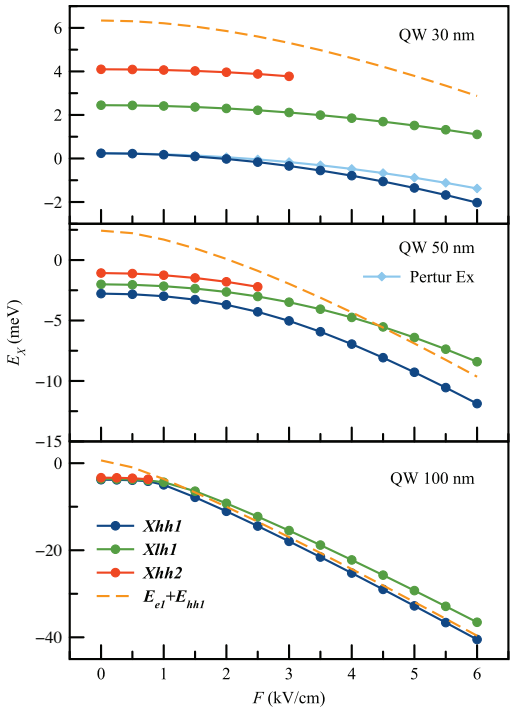

Fig. 1. The electric field dependence of exciton energies for different states in three QWs is shown by solid lines with symbols. The dashed curves represent the sum of the free electron and free heavy hole energies. The blue curve in the upper panel depicts the calculation within the framework of perturbation theory, including the Xhh1-Xhh2 coupling only.

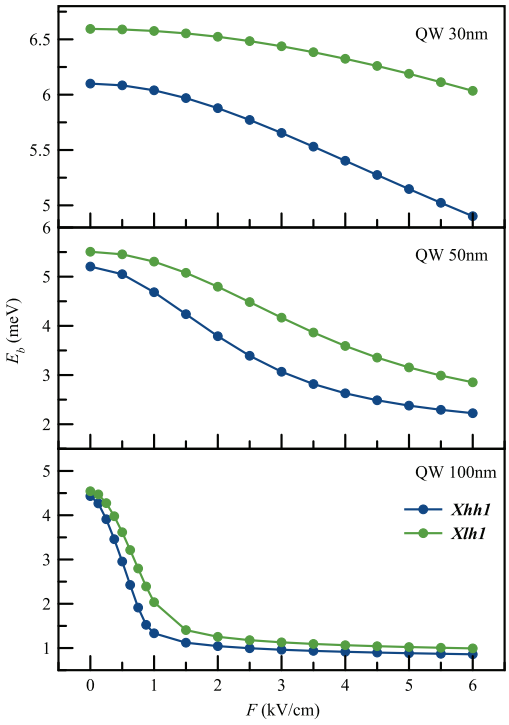

Fig. 2. Dependence of the binding energy of exciton states on the electric field in three QWs.

theory is applicable in the smaller electric field range, and the Xhh1-Xhh2 coupling describes, respectively, 47% and 7% of the Stark shift curvature coefficient.

When the exciton is stretched by the electric field, the distance between the electron and hole that constitute it gradually increases, causing the binding energy to gradually approach zero [19,56]. As seen in Fig. 1, the energy distance between the $E_e + E_{hh1}$ and E_X of Xhh1 curves gradually decreases with the electric field increase, which indicates the decrease of the binding energy. The dependencies of the binding energies of the Xhh1 and Xlh1 exciton states on the electric field are shown in Fig. 2 for all three QWs studied.

The decrease in binding energy varies for different QWs. It is small for the 30-nm QW and significantly larger for the wider QWs. Moreover, the binding energy decreases to a finite value rather than to zero, in the 100-nm QW. This phenomenon can be explained by the fact that the electron and the hole, which are moved apart from each other by the applied electric field, are confined by the QW boundaries. As a result, their Coulomb interaction remains finite.

$$E_C = \left\langle \psi(z_e, z_h, \rho) \left| \frac{q^2}{\varepsilon \cdot r} \right| \psi(z_e, z_h, \rho) \right\rangle. \tag{18}$$

The Coulomb energy obtained using the calculated wave functions for the Xhh1 and Xlh1 exciton states in the 100-nm QW in an electric field $F = 6$ kV/cm are, respectively, 1.27 meV and 1.37 meV. The low limit of the Coulomb energy for an electron and a hole as point charges at a distance $L = 100$ nm, $E_C = q^2/(\varepsilon L) = 0.98$ meV. The binding energy obtained in the exact numerical calculations for the 100-nm QW in a strong electric field, $F = 6$ kV/cm, is a bit smaller: $E_b = 0.86$ meV for the Xhh1 exciton state and $E_b = 0.99$ meV for the Xlh1 exciton state. This difference is explained by the contribution of kinetic energy, E_{kin}, of the charged carriers to the binding energy: $E_b = |-E_C + E_{kin}|$. Comparing these values, we can conclude that the kinetic energy has little effect on the binding energy of excitons in strong electric fields.

The effect of the QW boundaries is illustrated in Fig. 3 for the 100-nm QW in more detail. The figure shows the charged carrier density distributions. They are calculated by integrating the exciton wave function squared over the coordinate z of the other particle [70]. E.g., the expression for electron density distribution reads,

$$\rho_e = |\psi_e(z_e, \rho)|^2 = \int |\psi(z_e, z_h, \rho)|^2 dz_h. \tag{19}$$

A similar expression for the hole density distribution, ρ_h, is obtained by replacing indexes $e \leftrightarrow h$. It is worth noting that the exciton wave functions are normalized, $\langle \psi(z_e, z_h, \rho) | \psi(z_e, z_h, \rho) \rangle = 1$, so that the color in Fig. 3 reflects real density in units of nm^{-3}. As seen, when the applied electric field increases above 1.5 kV/cm, the electron and hole densities are concentrated near the QW boundaries and blocked by them. Correspondingly, the relative distance between the two charged carriers remains almost unchanged at large electric fields.

Fig. 3 also shows that the density distribution maximum of the heavy hole in the Xhh1 exciton state is closer to the QW boundary than that of the light hole in the Xlh1 exciton state. This is due to the fact that the quantization energy of a particle is inversely proportional to its effective mass. The electric field transforms the original rectangular QW potential into a triangular potential well [71]. Therefore, the wave function of the light hole with higher energy can be more widely distributed in the triangular QW. Similarly, the electron density is more widely distributed because the electron mass is smaller than the masses of the light and heavy holes.

4.2. Effect of external electric field on the exciton-light coupling

The ability of the exciton states (Xhh1, Xlh1, Xhh2) in a QW to couple with incident light changes when the states are stretched by an applied electric field. Using Eq. (12), we have modeled the influence of the electric field on the exciton-light coupling constant, $\hbar\Gamma_0$. Results are shown in Fig. 4. We have to note that the $\hbar\Gamma_0$ constant of the Xhh2 exciton state becomes unreliable when the external electric field F exceeds 3 kV/cm, 2.5 kV/cm, and 0.75 kV/cm in the 30-nm, 50-nm,

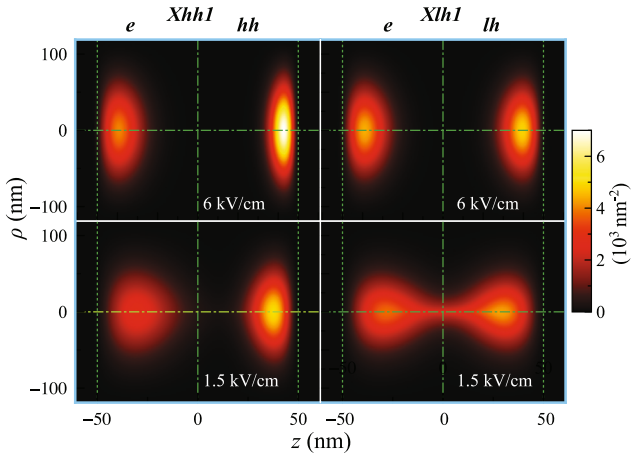

Fig. 3. The sum of the electron and hole density distributions for the Xhh1 and Xlh1 exciton states, $|\psi_e(z_e,\rho)|^2+|\psi_h(z_h,\rho)|^2$, in the 100-nm QW for the case of electric field $F = 1.5$ kV/cm (lower panels) and $F = 6$ kV/cm (upper panels). The calculation step is 1 nm.

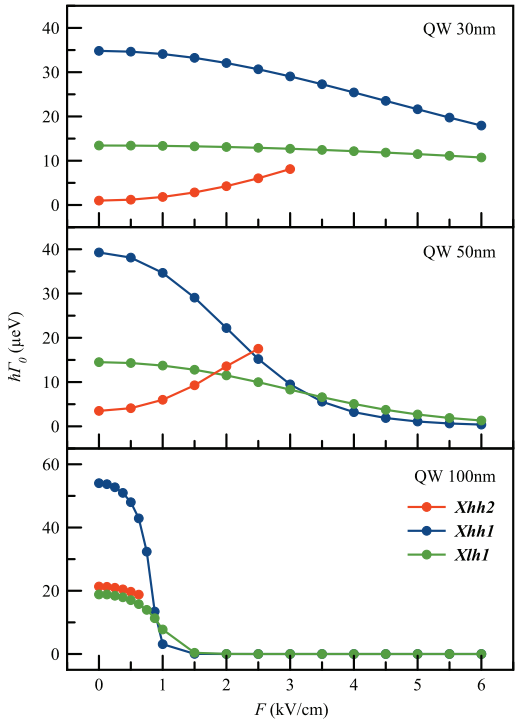

Fig. 4. Dependence of radiative broadening, $\hbar\Gamma_0$, on the applied electric field.

and 100-nm QWs, respectively. This is due to the overlap of this state with the continuum of states corresponding to uncoupled electron–hole pairs.

As shown in Fig. 4, the radiative broadening $\hbar\Gamma_0$ of the Xhh1 and Xlh1 exciton states decreases with increasing external electric field. This effect is most prominent in the case of the 100-nm QW. The exciton-light coupling for the Xhh1 state decreases from $\hbar\Gamma_0 = 54$ μeV to 0.04 μeV, and for the Xlh1 state, it decreases from 19 μeV to 0.4 μeV even at a small electric field of 1.5 kV/cm. According to Fig. 3, this is due to rapid decrease of the probability of the electron and the hole to be located at the same point in space, which determines the exciton-light coupling [see Eq. (12)]. However, the behavior of $\hbar\Gamma_0$ for the Xhh2 exciton state differs significantly. Namely, $\hbar\Gamma_0$ gradually increases for the 30-nm and 50-nm QWs as the external electric field

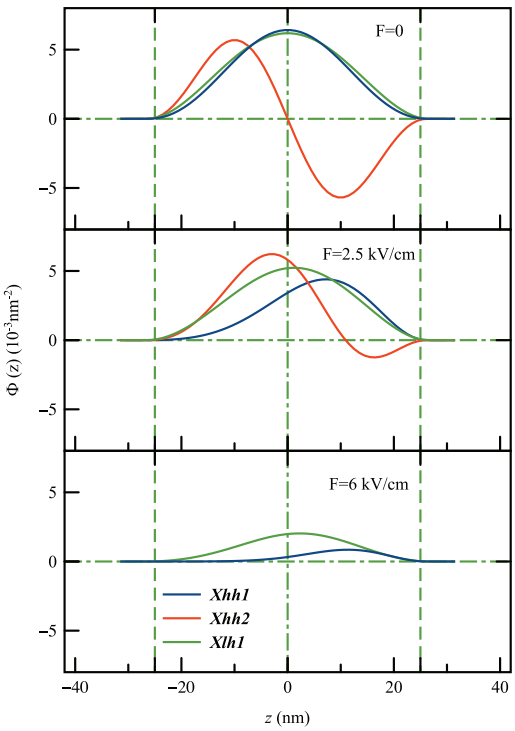

Fig. 5. The cross section $\Phi(z)$ of wave functions of the Xhh1, Xlh1, and Xhh2 exciton states in the 50-nm QW in different electric fields indicated in the panels.

increases. For the 100-nm QW, it remains almost constant in the electric fields studied.

The theoretically obtained phenomena are consistent with those experimentally observed in Ref. [24] for radiative broadening of exciton states in a 30-nm QW in external electric fields. According to this work, the radiative broadening of the Xhh1 and Xlh1 exciton states does decrease with increasing external electric field. This is consistent with the results shown in Fig. 3. For the case of Xhh2 exciton state, the experimentally obtained radiative broadening increases with increasing electric field, which is also consistent with our calculations.

Let us analyze the theoretically predicted behavior of exciton-light coupling in a more quantitative manner. According to Eq. (12), the exciton-light coupling is determined by the overlap of the function $\Phi(z)$ with the plane wave e^{iqz} describing the incident light wave. The squared integral can be expressed as:

$$\begin{aligned}\left|\int_{-\infty}^{\infty}\phi(z)e^{ikz}dz\right|^2 &= |I_C|^2+|I_S|^2\\ &\equiv\left|\int_{-\infty}^{\infty}\Phi(z)\cdot\cos(kz)dz\right|^2+\left|\int_{-\infty}^{\infty}\Phi(z)\cdot\sin(kz)dz\right|^2.\end{aligned}\tag{20}$$

Functions $\Phi(z)$ for the Xhh1 and Xlh1 exciton states are symmetric relative to the QW center in the absence of an electric field. Accordingly, only the first term in Eq. (20), $|I_C|^2$, contributes to $\hbar\Gamma_0$. When the electric field is applied, functions $\Phi(z)$ are distorted, and both terms, $|I_C|^2$ and $|I_S|^2$, become non-zero. Examples of the $\Phi(z)$ functions of the Xhh1 state under different electric fields for the 50-nm QW are shown in Fig. 5. However, the amplitude of $\Phi(z)$ significantly decreases in strong electric fields (see an example in the lower panel of Fig. 5). This is due to the reduced overlap of the electron and hole density distributions, as illustrated in Fig. 3. This effect leads to significant drops in $\hbar\Gamma_0$.

The behavior of the exciton-light coupling of the Xhh2 state shown in Fig. 4 can be understood considering again Eq. (12) and the profile of the function for this state. At zero electric field, the function $\Phi(z)$ is antisymmetric with respect to the QW center (see Fig. 5). Consequently,

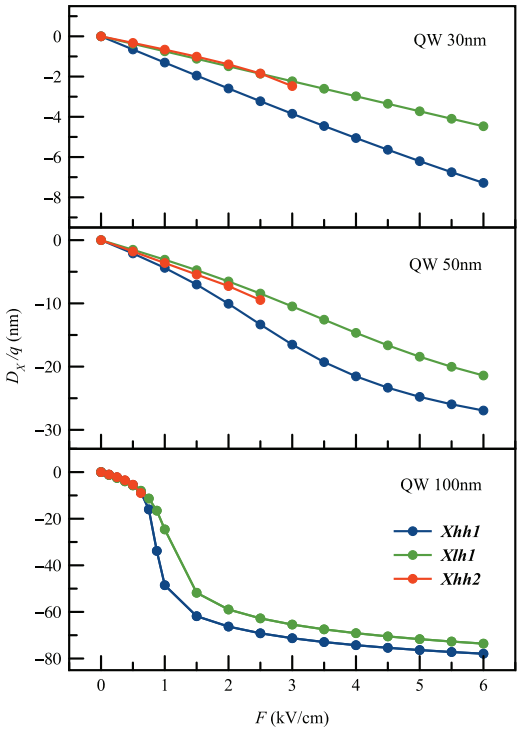

Fig. 6. Dependence of the exciton dipole moment on the applied electric field.

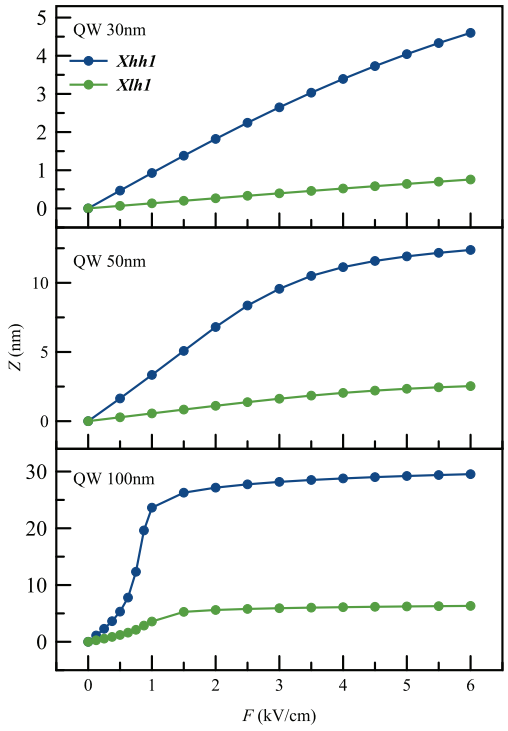

Fig. 7. Electric field dependence of the center of mass position of exciton states in separate QWs of different widths.

only the second term, $|I_S|^2$, of Eq. (20) contributes to $\hbar\Gamma_0$. This contribution is relatively small for the 30-nm and 50-nm QWs due to the small QW width compared to the light wavelength. In the 100-nm QW, the contribution is significantly greater due to the larger overlap between $\Phi(z)$ and the light wave. When the electric field is applied, the function $\Phi(z)$ is modified as shown in Fig. 5. Accordingly, the overlap integral I_C starts to grow, which results in an overall increase of the exciton-light coupling in the 30-nm and 50-nm QWs. However, in the case of the 100-nm QW, the increase in integral I_C is compensated by the rapid decrease of integral I_S. As a result, $\hbar\Gamma_0$ remains almost unchanged within the studied electric field range.

4.3. Exciton dipole moment in external electric field

As mentioned above, the static dipole moment of the exciton state is proportional to the average distance between the electron and the hole in the exciton. In the individual QWs considered in this study, the static dipole moments of all three exciton states gradually increase in absolute value from zero as the electric field increases (see Fig. 6). The negative values in Fig. 6 merely indicate the direction of the dipole moment. In narrower QWs, the exciton is stronger confined by the QW boundaries. Consequently, the dipole moments of all the exciton states increase linearly but at a slower rate in the 30-nm QW. The maximum value of D_X/q, the dipole moment in units of the electron charge, is only -7 nm for the Xhh1 state and approximately -4 nm for the Xlh1 state, which is significantly smaller than the exciton Bohr radius ($a_B \approx 15$ nm).

When the QW width increases to 50 nm, the exciton state becomes more sensitive to the electric field. For $F \geq 4$ kV/cm, the dipole moment of the Xhh1 exciton state begins to change nonlinearly with increasing electric field. This means that the electron and hole in the exciton state are spatially separated and confined by the QW boundaries. When the QW width reaches 100 nm, even in a weak electric field, $F = 1.5$ kV/cm, the electron and the hole in the Xhh1 and Xlh1 exciton states move close to the QW boundaries (see Fig. 3). The mean distance between the electron and hole becomes large, $|D_X/q| > 50$ nm, which is greater than the exciton Bohr radius. Further substantial increase in the dipole moment is limited by the QW boundaries. This behavior of the dipole moment is consistent with that of the exciton energy E_X, the exciton binding energy E_b, and the radiative broadening $\hbar\Gamma_0$, as shown in Figs. 1, 2, and 4, respectively.

4.4. Shift of exciton center of mass in electric field

Due to the difference in effective masses of an electron and a hole, the application of an electric fields leads to a displacement of the center of mass of excitons. This effect is described by Eq. (15). The greater the difference between the masses of charged carriers, the greater the shift Z is expected to be. Here, we have calculated the center of mass position for the Xhh1 and Xlh1 exciton states in all three QWs under an applied external electric field. The results are shown in Fig. 7.

As seen in the figure, the shift Z of the heavy-hole and light-hole excitons differs significantly in all three QWs. In the 30-nm QW, it is nearly linear in the electric fields studied and relatively small compared to the QW width. At the same time, the Xhh1 exciton shift is approximately 6 times greater than that of the Xlh1 exciton state. For the 50-nm QW, the shift of the Xhh1 exciton becomes sublinear for $F > 3$ kV/cm, while the Xlh1 exciton position remains almost linearly dependent on the electric field. The ratio of the exciton shifts, $R = Z_{Xhh1}/Z_{Xlh1} = 4.9$, for $F = 6$ kV/cm. In the case of the 100-nm QW, the shifts of both excitons increase slowly for electric fields $F > 1.5$ kV/cm, and their ratio, $R = 4.7$, at $F = 6$ kV/cm. The strong shift of the heavy-hole exciton, compared to that of the light-hole exciton, is associated with a stronger localization of the heavy-hole exciton, rather than with the large ratio of their masses, which is only 2.66.

The observed nonlinear behavior of the exciton center-of-mass shift is consistent with the behavior of other exciton characteristics shown in Figs. 2, 4, and 6. It is instructive again to evaluate the maximum shift of the exciton center of mass considering the electron and the hole as point charges. In strong electric fields, they are located near the QW boundaries, that is, $z_e = -50$ nm and $z_h = 50$ nm in the 100-nm QW. Simple calculations show that the center of mass positions of

the Xhh1 and Xlh1 exciton states are, respectively, 34 nm and 7.3 nm. These values are close to those obtained from the exact numerical calculations, $Z_{Xhh1} = 29.5$ nm and $Z_{Xlh1} = 6.32$ nm, for the 100-nm QW.

5. Modeling of reflection spectra

The properties of exciton states in QW heterostructures can be studied in experiments through their reflection spectra [12,24]. The exciton characteristics calculated in previous sections allow us to the model reflection spectra, which could be observed experimentally.

According to the nonlocal dielectric response theory [1], the intensity reflection coefficient, R, of a QW heterostructure can be expressed as follows:

$$R(\hbar\omega) = \left| \frac{r_s + r_{QW}(\hbar\omega)}{1 + r_s \cdot r_{QW}(\hbar\omega)} \right|^2. \tag{21}$$

Here, r_s is the amplitude reflection from the surface of the heterostructure sample, r_{QW} is the amplitude reflection of the QW, and $\hbar\omega$ is the photon energy of the incident light.

The amplitude reflection r_s weakly depends on the photon energy and can be considered constant for the GaAs surface in the spectral range under study [59], $r_s \approx -0.565$. The amplitude reflection r_{QW} is a sum of resonant terms. Each term depends on the energy E_{Xj} of the exciton resonance j, the radiative broadening $\hbar\Gamma_{0j}$, the nonradiative broadening $\hbar\Gamma_j$, and the phase ϕ_j:

$$r_{QW}(\hbar\omega) = \sum_j \frac{i\hbar\Gamma_{0j} e^{i2\phi_j}}{(E_g + E_{Xj}) - \hbar\omega - i\hbar(\Gamma_j + \Gamma_{0j})}. \tag{22}$$

Here $E_g = 1519.4$ meV is the band gap energy of GaAs [21] and index $j = 1, 2, 3, \ldots$ enumerates exciton states.

The parameter $\hbar\Gamma_j$ in Eq. (22) represents the nonradiative broadening of the exciton resonance. It phenomenologically describes the contribution of all broadening mechanisms of the exciton resonance, which are always observed in experiments [72]. In high-quality heterostructures, the inhomogeneous part of the broadening is negligible, so we can consider only the homogeneous nonradiative broadening. The latter is related to the interaction of excitons with other quasiparticles in the system, such as phonons, other excitons, and free charge carriers [73]. This interaction is unavoidable in real structures and we assume a finite value for the broadening, $\hbar\Gamma_j = 120$ μeV for the 30-nm and 50-nm QWs and 60 μeV for the 100-nm QW. The smaller value of $\hbar\Gamma_j$ for the widest QW is consistent with experimental observations [20,21]. Another possible mechanism for the nonradiative broadening could be, in principle, related to the carrier tunneling through barrier layers in the presence of an electric field. However, we ignore this broadening mechanism by assuming sufficiently high potential barriers. Correspondingly, we ignore any dependence of $\hbar\Gamma_j$ on the electric field strength [74].

The parameter ϕ_j, which represents the phase of an exciton resonance, is given by the following expression [24,59]:

$$\tan(\phi_j) = \frac{\int \Phi_j(z)\sin(kz)dz}{\int \Phi_j(z)\cos(kz)dz} \equiv \frac{I_{Sj}}{I_{Cj}}. \tag{23}$$

Besides the phase ϕ_j, which is determined by the symmetry of the exciton wave function, there is another phase, ϕ_0, which can modify the profile of exciton resonances [20]. This phase shift results from the propagation of the light wave through a top layer (up to the middle of the QW [1]), which separate the surface of the structure from the QW, $\phi_0 = 2\pi[L_{\text{top}}/(\lambda/n_{\text{top}})]$. Here L_{top} is the thickness of the top layer, λ is the wavelength of light, and n_{top} is the effective refractive index of the top layer. For simplicity, we assume that the top layer thickness is chosen so that $[L_{\text{top}}/(\lambda/n_{\text{top}})] = 1$. In this case, $\phi_0 = 2\pi$, and it does not affect the exciton resonances.

Examples of reflection spectra calculated using Eqs. (21)–(23) are shown in Fig. 8. As seen in the upper panels, the Xhh1 resonance at zero

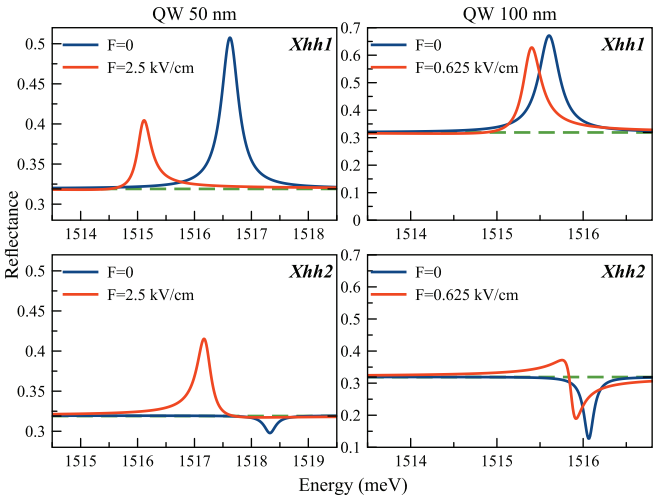

Fig. 8. Examples of reflection spectra in the range of the Xhh1 and Xhh2 resonances in the 50-nm (left panels) and 100-nm (right panels) QWs at zero and some electric fields indicated in the panels. The spectra are calculated using Eqs. (21)–(23) and numerical results shown in Figs. 1 and 4. The dashed lines show the background reflection from the heterostructure surface, $|r_s|^2 \approx 0.32$.

electric field manifests itself as a Lorentzian peak superimposed on the background reflection, $R_s = |r_s|^2$, from the heterostructure surface. For the GaAs surface, value of $R_s \approx 0.32$. The full width at half maximum (FWHM) of the Lorentzian peak, ΔE, is determined by the radiative $\hbar\Gamma_0$ and non-radiative $\hbar\Gamma$ broadenings of the exciton resonance, as well as by the amplitude reflection $|r_s|$, $\Delta E = 2\hbar[(\Gamma_0 + \Gamma) + |r_s|\Gamma_0]$ [20]. The phase ϕ of the resonance is zero because the function $\Phi(z)$ is symmetric relative to the QW center (see Fig. 5) and the overlap integral $I_S = 0$, see Eq. (23).

When the electric field is applied, the resonance shifts to the lower energy region (the Stark shift) and its amplitude decreases. The latter is due to a decrease of the exciton-light coupling strength $\hbar\Gamma_0$, as shown in Fig. 4. In addition, the peak acquires an asymmetric shape with a high-energy tail. This is related to the field-induced modification of the function $\Phi(z)$ of this resonance shown in Fig. 5. The phase of the resonance becomes non-zero. In particular, the phase changes from 0 to −0.26 rad for the 50-nm QW and to −0.43 rad for the 100-nm QW in the electric fields indicated in Fig. 8. We should note that the phase of the Xlh1 resonance is less sensitive to the electric field and varies only from 0 to −0.04 rad and −0.05 rad, respectively, in the considered cases. Therefore the asymmetry of this resonance is almost invisible, and we do not show it in this figure. The smaller change of phase for the Xlh1 resonance is explained by smaller shift of its center of mass, see Fig. 7. The calculated changes of phases are similar to the experimental results presented in Ref. [24].

The phase ϕ_j of the Xhh2 resonance is much more sensitive to the electric field. The bottom panels of Fig. 8 illustrate this sensitivity. At zero electric field, the resonance is observed as a dip with the amplitude determined by the radiative broadening shown in Fig. 4. The phase of this resonance, $\phi = \pi$, which is due to the odd symmetry of its function $\Phi(z)$, as shown in Fig. 5. The FWHM of the dip, $\Delta E = 2\hbar[(\Gamma_0 + \Gamma) - |r_s|\Gamma_0]$, which is noticeably smaller than that for the peak with the same exciton parameters [20].

In the presence of an electric field, the function $\Phi(z)$ of the Xhh2 state is modified as shown in the middle panel of Fig. 5. Correspondingly, the overlap integral I_C increases while the integral I_S decreases, which results in a decrease in the phase ϕ. When the electric field becomes strong enough (see the left bottom panel in Fig. 8), the Xhh2 resonance transforms from the dip to a peak with a low-energy tail. The phase of this resonance, $\phi \approx -0.16$ rad, which is close to zero. In the case of the 100-nm QW, we managed to calculate parameters

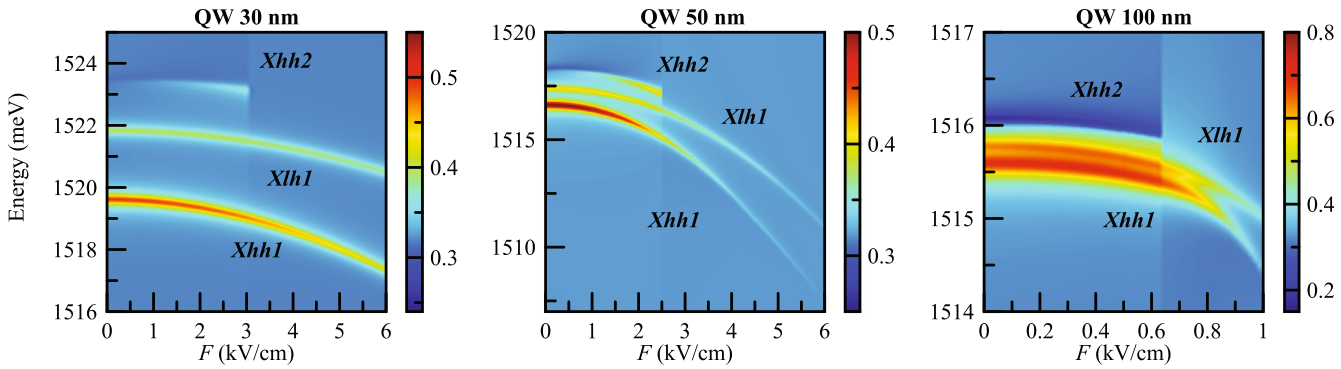

Fig. 9. Reflection spectra modeled for the QW widths of 30, 50, and 100 nm. The exciton states Xhh1, Xlh1, and Xhh2 are taken into account.

of the Xhh2 exciton only for the relatively small electric fields up to $F = 0.625$ kV/cm at most (see Figs. 1–4). The resonance transforms under such a field into a dispersion-like curve with long tails in the lower and higher energy regions. The phase $\phi \approx -1.08$ rad in this case.

To summarize the results of the theoretical study of the excitons, we have modeled reflection spectra of heterostructures with three QWs in the whole range of electric field considered. The discrete numerical data for the exciton energies E_X and radiative broadening $\hbar\Gamma_0$ shown in Figs. 1 and 4, respectively, were interpolated to obtain smooth dependencies on the electric field. For the Xhh2 exciton states, we used only the data reliably obtained in the calculations in the limited ranges of the electric field, $F < 3$ kV/cm for the 30-nm QW, $F < 2.5$ kV/cm for the 50-nm QW, and $F < 0.625$ kV/cm for the 100-nm QW. The modeled reflection spectra are shown in Fig. 9. The light blue color in the figure represents the background reflection from the heterostructure surface. The exciton states in reflection spectra are represented as resonant features. These resonances are depicted in the green to red colors when they have a peak-like shape with an increased reflection coefficient and in dark blue for the dip in the reflection.

The Xhh1 and Xlh1 exciton resonances are represented as reflection peaks. The Stark shift of these resonances reproduces that shown in Fig. 1. However, their visibility rapidly decreases with the electric field increase, in particular, for the 50-nm and 100-nm QWs. This is due to the electric-field-induced decrease of the exciton-light coupling strength shown in Fig. 4. These resonances become nearly invisible for the 100-nm QW at electric field $F > 1$ kV/cm. Therefore, this field range is not shown in the right panel of Fig. 9. The visibility of these resonances in experiments can drop even faster because of an additional nonradiative broadening of the resonances with the increase of the electric field [24]. The Xhh1 and Xlh1 resonances can overlap in the 100-nm QW due to the nonradiative broadening.

The Xhh2 exciton resonance in the studied QWs appears in the reflection spectra differently from the Xhh1 and Xlh1 resonances. At small electric fields, the Xhh2 state is observed as a reflection dip for all three QWs. For example, the reflection coefficient for a heterostructure with the 100-nm QW at the Xhh2 exciton resonance is about 0.18 at $F = 0$ kV/cm. When the external electric field gradually increases, the Xhh2 resonance is transformed into a peak. The maximum amplitude of the Xhh2 resonant reflection reaches 0.42 for the 50-nm QW in the electric field of 2.5 kV/cm. It may increase further in larger electric fields, but we have not been able to reliably calculate the characteristics of the Xhh2 exciton for such electric fields.

In the heterostructure with the 100-nm QW, the Xhh2 resonance is observed as a dip at zero field and transforms into a dispersion-like curve with the field increase (compare with Fig. 8). Due to the dispersion-like shape of the resonance, its wings are seen far from the Xhh2 exciton energy. In particular, these wings are visible in the right panel of Fig. 9 as a dark (light) blue area in the high (low) energy region for the electric fields $F < 0.625$ kV/cm. We did not manage to study the Xhh2 exciton at fields $F > 0.625$ kV/cm, so its contribution is not represented in this electric field region, which leads to a sharp color change in the figure.

The general shape of the exciton resonance reflection for a heterostructure with the 50-nm QW is similar to that for the 30-nm QW, which indicates a gradual change in the characteristics of exciton states from those in a relatively narrow QW to those in a wide QW.

6. Conclusion

We used the fourth-order finite difference method to accurately solve the Schrödinger equation that describes the quantum mechanical behavior of exciton states (Xhh1, Xlh1, and Xhh2) in the $GaAs/Al_xGa_{1-x}As$ ($x = 0.3$) QWs with widths of 30, 50, and 100 nm in an external electric field applied along the structure axis. The Stark shift of exciton states is found to gradually increase from a few units of meV in the 30-nm QW to several tens of meV in the 100-nm QW at $F = 6$ kV/cm. Under small electric fields, the Stark shift can be described by perturbation theory. The Xhh2 state was studied in a smaller range of electric fields. At large electric fields, for example, at $F > 3$ kV/cm for the 30-nm QW, it overlaps with a continuous spectrum of states of the free electrons and holes and cannot be found by the numerical algorithm used.

The binding energy of the Xhh1 and Xlh1 gradually decreases as the external electric field increases from 0 to 6 kV/cm. This decrease is more pronounced for the widest QW. For the 100-nm QW, an abrupt, threshold-like, decrease in the binding energy is observed in the electric fields of $0.5 \to 1$ kV/cm. This behavior indicates a break in the Coulomb coupling of the electron and the hole in the exciton, i.e., dissociation of the exciton. At the same time, the binding energy decreases down to a non-zero value of about 1 meV, rather than reaching zero. This is due to the blocking effect of the QW boundaries when the average distance between the electron and the hole inside the exciton cannot exceed the width of the QW.

The applied electric field polarizes the excitons. The static dipole moment of the Xhh1 and Xlh1 excitons increases linearly (in absolute value) in the 30-nm QW and experiences an abrupt increase at $F \approx 1$ kV/cm in the 100-nm QW. Then the dipole moment remains almost constant at larger electric fields in this QW, which is also due to the blocking effect of the QW boundaries.

The exciton-light coupling constant $\hbar\Gamma_0$ of the Xhh1 and Xlh1 states gradually decreases in the narrow QW and decreases abruptly down to zero at $F > 1$ kV/cm in the 100-nm QW. This indicates a strong decrease in the overlap of the electron and hole densities in the excitons induced by the exciton polarization. The exciton-light coupling constant of the Xhh2 state is small for the narrow QW and comparable to that of the Xlh1 state for the 100-nm QW in the absence of the electric field. This constant increases with the electric field increase in the 30-nm and 50-nm QWs and remains almost constant in the 100-nm QW. This behavior is explained by specific features of the overlap of the sine-like and cosine-like parts of the light wave with the Xhh2 exciton

state, whose wave function is antisymmetric at zero field and is strongly modified when the electric field is applied.

The applied electric field shifts the center of mass of the excitons, although the exciton is a neutral quasi-particle. This effect is caused by a difference in the masses of the electron and the hole in the exciton. The heavy hole/electron mass ratio, $m_{hh}/m_e = 5.2$, which is several times larger than that for the light hole/electron masses ($m_{lh}/m_e = 1.34$). Therefore, the shift of the center of mass of a heavy-hole exciton with an increase in the field occurs several times more strongly for all three QWs. For a wide QW (100 nm), the threshold behavior of the effect is again observed in the field $F = 1$ kV/cm, above which the displacement of the center of mass slows down. This is also explained by the limitation of the movement of the electron and the hole in the QW.

The obtained results enabled us to model reflection spectra, which can be observed experimentally. The modeling shows that the visibility of exciton resonances gradually decreases with the increase of the electric field, in particular, for wide QWs. For the 100-nm QWs, the resonances are hardly visible at electric fields $F > 1$ kV/cm.

CRediT authorship contribution statement

Shiming Zheng: Writing – original draft, Software, Investigation, Formal analysis. **E.S. Khramtsov:** Writing – original draft, Software, Investigation. **I.V. Ignatiev:** Writing – review & editing, Writing – original draft, Supervision, Investigation, Conceptualization.

Ethical compliance

The research meets all applicable standards for the ethics of experimentation and research integrity.

Funding

Financial support from the Russian Science Foundation, Russia, grant No. 19-72-20039, is acknowledged. E. S. Khramtsov acknowledges the Saint-Petersburg State University, Russia for the financial support of numerical simulations, grant No. 125022803069-4. Shiming Zheng would like to thank the support from China Scholarship Council, China.

Declaration of competing interest

The authors declare that they have no known competing financial interests or personal relationships that could have appeared to influence the work reported in this paper.

Acknowledgments

The authors thank P. A. Belov, M. A. Chukeev and D. K. Loginov for fruitful discussions and A. Levantovsky for providing the advanced plotting and curve fitting program MagicPlot. Research was carried out using computational resources provided by "Computer Center of SPbU" Resource Center (http://www.cc.spbu.ru/en).

Data availability

The authors are unable or have chosen not to specify which data has been used.

References

[1] E.L. Ivchenko, Optical Spectroscopy of Semiconductor Nanostructures, Alpha Science International, Ltd, 2005.
[2] A. Kavokin, J. Baumberg, G. Malpuech, F. Laussy, Microcavities, in: Series on Semiconductor Science and Technology, OUP Oxford, 2007.
[3] C.F. Klingshirn, Semiconductor Optics, Springer Berlin Heidelberg, 2012.
[4] N. Tomassini, A. D'Andrea, R. Del Sole, H. Tuffigo-Ulmer, R.T. Cox, Center-of-mass quantization of excitons in CdTe/$Cd_{1-x}Zn_xTe$ quantum wells, Phys. Rev. B 51 (8) (1995) 5005–5012.
[5] E.S. Khramtsov, P.A. Belov, P.S. Grigoryev, I.V. Ignatiev, S.Y. Verbin, Y.P. Efimov, S.A. Eliseev, V.A. Lovtcius, V.V. Petrov, S.L. Yakovlev, Radiative decay rate of excitons in square quantum wells: Microscopic modeling and experiment, J. Appl. Phys. 119 (2016) 184301.
[6] A. Tredicucci, Y. Chen, F. Bassani, J. Massies, C. Deparis, G. Neu, Center-of-mass quantization of excitons and polariton interference in GaAs thin layers, Phys. Rev. B 47 (16) (1993) 10348–10357.
[7] E. Ubyivovk, Y. Dolgikh, Y. Efimov, S. Eliseev, I. Gerlovin, I. Ignatiev, V. Petrov, V. Ovsyankin, Spectroscopy of high-energy excitonic states in ultra-thick GaAs quantum wells with a perfect crystal structure, J. Lumin. 102–103 (2003) 751–754.
[8] S. Schumacher, G. Czycholl, F. Jahnke, I. Kudyk, H.I. Rückmann, J. Gutowski, A. Gust, G. Alexe, D. Hommel, Polariton propagation in shallow-confinement heterostructures: Microscopic theory and experiment showing the breakdown of the dead-layer concept, Phys. Rev. B 70 (23) (2004) 235340.
[9] M. Nakayama, D. Kim, H. Ishihara, Center-of-mass quantization of excitons in PbI_2 thin films grown by vacuum deposition, Phys. Rev. B 74 (7) (2006) 073306.
[10] D. Schiumarini, N. Tomassini, L. Pilozzi, A. D'Andrea, Polariton propagation in weak-confinement quantum wells, Phys. Rev. B 82 (7) (2010) 075303.
[11] A.V. Trifonov, S.N. Korotan, A.S. Kurdyubov, I.Y. Gerlovin, I.V. Ignatiev, Y.P. Efimov, S.A. Eliseev, V.V. Petrov, Y.K. Dolgikh, V.V. Ovsyankin, A.V. Kavokin, Nontrivial relaxation dynamics of excitons in high-quality InGaAs/GaAs quantum wells, Phys. Rev. B 91 (11) (2015) 115307.
[12] E.S. Khramtsov, P.S. Grigoryev, D.K. Loginov, I.V. Ignatiev, Y.P. Efimov, S.A. Eliseev, P.Y. Shapochkin, E.L. Ivchenko, M. Bayer, Exciton spectroscopy of optical reflection from wide quantum wells, Phys. Rev. B 99 (3) (2019) 035431.
[13] G. Bastard, E.E. Mendez, L.L. Chang, L. Esaki, Exciton binding energy in quantum wells, Phys. Rev. B 26 (4) (1982) 1974–1979.
[14] R.L. Greene, K.K. Bajaj, D.E. Phelps, Energy levels of wannier excitons in GaAs - $Ga_{1-x}Al_xAs$ quantum-well structures, Phys. Rev. B 29 (4) (1984) 1807–1812.
[15] R. Miller, D. Kleinman, Excitons in GaAs quantum wells, J. Lumin. 30 (1–4) (1985) 520–540.
[16] L.C. Andreani, A. Pasquarello, Accurate theory of excitons in GaAs-$Ga_{1-x}Al_xAs$ quantum wells, Phys. Rev. B 42 (14) (1990) 8928–8938.
[17] R. Winkler, Excitons and fundamental absorption in quantum wells, Phys. Rev. B 51 (20) (1995) 14395–14409.
[18] H.M. Gibbs, G. Khitrova, S.W. Koch, Exciton–polariton light–semiconductor coupling effects, Nat. Photonics 5 (5) (2011) 273–273.
[19] P. Belov, Energy spectrum of excitons in square quantum wells, Phys. E 112 (2019) 96–108.
[20] P.Y. Shapochkin, S. Eliseev, V. Lovtcius, Y.P. Efimov, P. Grigoryev, E. Khramtsov, I. Ignatiev, Excitonic probe for characterization of high-quality quantum-well heterostructures, Phys. Rev. Appl. 12 (3) (2019) 034034.
[21] M.N. Bataev, M.A. Chukeev, M.M. Sharipova, P.A. Belov, P.S. Grigoryev, E.S. Khramtsov, I.V. Ignatiev, S.A. Eliseev, V.A. Lovtcius, Y.P. Efimov, Heavy-hole–light-hole exciton system in GaAs/AlGaAs quantum wells, Phys. Rev. B 106 (8) (2022) 085407.
[22] L. Butov, Excitonic devices, Superlattices Microstruct. 108 (2017) 2–26.
[23] C.J. Dorow, M.W. Hasling, D.J. Choksy, J.R. Leonard, L.V. Butov, K.W. West, L.N. Pfeiffer, High-mobility indirect excitons in wide single quantum well, Appl. Phys. Lett. 113 (21) (2018) 212102–1–212102–5.
[24] M.A. Chukeev, S. Zheng, E.S. Khramtsov, I.V. Ignatiev, S.A. Eliseev, V.A. Lovtcius, Y.P. Efimov, M.A. Lozhkin, Excitonic sensor of electric field in quantum-well heterostructures, Phys. Rev. B 109 (23) (2024) 235305.
[25] D.A. Baghdasaryan, E.S. Hakobyan, D.B. Hayrapetyan, I.V. Iorsh, I.A. Shelykh, V. Shahnazaryan, Tunable strongly interacting dipolar excitons in hybrid perovskites, Phys. Rev. Mater. 6 (3) (2022) 034003.
[26] N. Scheuler, P. Rommel, J. Main, P.A. Belov, Resonance energies and linewidths of Rydberg excitons in Cu_2O quantum wells, Phys. Rev. B 109 (16) (2024) 165440.
[27] P.A. Belov, F. Morawetz, S.O. Krüger, N. Scheuler, P. Rommel, J. Main, H. Giessen, S. Scheel, Energy states of Rydberg excitons in finite crystals: From weak to strong confinement, Phys. Rev. B 109 (23) (2024) 235404.
[28] J. Heckötter, A. Farenbruch, D. Fröhlich, M. Aßmann, D. Yakovlev, M. Bayer, M. Semina, M. Glazov, P. Rommel, J. Ertl, J. Main, H. Stolz, The energy level spectrum of the yellow excitons in cuprous oxide, Phys. Rep. 1100 (2025) 1–69.
[29] E.E. Mendez, G. Bastard, L.L. Chang, L. Esaki, H. Morkoc, R. Fischer, Effect of an electric field on the luminescence of GaAs quantum wells, Phys. Rev. B 26 (12) (1982) 7101–7104.

[30] D.A.B. Miller, D.S. Chemla, T.C. Damen, A.C. Gossard, W. Wiegmann, T.H. Wood, C.A. Burrus, Band-edge electroabsorption in quantum well structures: The quantum-confined Stark effect, Phys. Rev. Lett. 53 (1984) 2173–2176.
[31] M. Matsuura, T. Kamizato, Subbands and excitons in a quantum well in an electric field, Phys. Rev. B 33 (12) (1986) 8385.
[32] B. Zhu, Exciton spectra in GaAs/$Ga_{1-x}Al_x$As quantum wells in an externally applied electric field, Phys. Rev. B 38 (18) (1988) 13316–13322.
[33] R.P. Leavitt, Empirical two-band model for quantum wells and superlattices in an electric field, Phys. Rev. B 44 (20) (1991) 11270–11280.
[34] S. Fafard, E. Fortin, J. Merz, Excitation-intensity-dependent photoluminescence quenching due to electric-field screening by photocarriers captured in single-quantum-well structures, Phys. Rev. B 48 (15) (1993) 11062.
[35] F. Bassani, G. Czajkowski, M. Dressler, L. Silvestri, Electro-optical properties of excitons in low-dimensional semiconductor structures, Phys. Status Solidi A 178 (1) (2000) 51–55.
[36] E.I. Rashba, A.L. Efros, Efficient electron spin manipulation in a quantum well by an in-plane electric field, Appl. Phys. Lett. 83 (25) (2003) 5295–5297.
[37] Y.-H. Kuo, Y.K. Lee, Y. Ge, S. Ren, J.E. Roth, T.I. Kamins, D.A.B. Miller, J.S. Harris, Strong quantum-confined Stark effect in germanium quantum-well structures on silicon, Nature 437 (7063) (2005) 1334–1336.
[38] L. Zhang, H.-Z. Duan, X.-F. Wang, Electric field effects on the states of an exciton in square cross-section quantum well wires, Phys. Lett. A 373 (33) (2009) 2969–2972.
[39] J. Kim, T. Kim, K. Yoo, Interband Stark effects in $In_xGa_{1-x}As/In_yAl_{1-y}As$ coupled step quantum wells, Appl. Surf. Sci. 240 (1–4) (2005) 452–455.
[40] A.V. Gorbunov, V.B. Timofeev, D.A. Demin, Electro-optical trap for dipolar excitons in a GaAs/AlAs Schottky diode with a single quantum well, JETP Lett. 94 (11) (2012) 800–805.
[41] K. Sivalertporn, L. Mouchliadis, A.L. Ivanov, R. Philp, E.A. Muljarov, Direct and indirect excitons in semiconductor coupled quantum wells in an applied electric field, Phys. Rev. B 85 (4) (2012) 045207.
[42] J. Wilkes, E.A. Muljarov, Exciton effective mass enhancement in coupled quantum wells in electric and magnetic fields, New J. Phys. 18 (2) (2016) 023032.
[43] J. Wilkes, E. Muljarov, Excitons and polaritons in planar heterostructures in external electric and magnetic fields: A multi-sub-level approach, Superlattices Microstruct. 108 (2017) 32–41.
[44] D.K. Loginov, P.A. Belov, V.G. Davydov, I.Y. Gerlovin, I.V. Ignatiev, A.V. Kavokin, Y. Masumoto, Exciton-polariton interference controlled by electric field, Phys. Rev. Res. 2 (3) (2020) 033510.
[45] J.J. Davies, D. Wolverson, V.P. Kochereshko, A.V. Platonov, R.T. Cox, J. Cibert, H. Mariette, C. Bodin, C. Gourgon, E.V. Ubyivovk, Y.P. Efimov, S.A. Eliseev, Motional enhancement of exciton magnetic moments in zinc-blende semiconductors, Phys. Rev. Lett. 97 (18) (2006) 187403.
[46] A. Arora, A. Mandal, S. Chakrabarti, S. Ghosh, Magneto-optical Kerr effect spectroscopy based study of Landé g-factor for holes in GaAs/AlGaAs single quantum wells under low magnetic fields, J. Appl. Phys. 113 (21) (2013) 213505.
[47] W. Bardyszewski, S.P. Łepkowski, Nonlinear Zeeman splitting of magnetoexcitons inc-plane wurtzite GaN-based quantum wells, Phys. Rev. B 90 (7) (2014) 075302.
[48] P.S. Grigoryev, O.A. Yugov, S.A. Eliseev, Y.P. Efimov, V.A. Lovtcius, V.V. Petrov, V.F. Sapega, I.V. Ignatiev, Inversion of Zeeman splitting of exciton states in InGaAs quantum wells, Phys. Rev. B 93 (20) (2016) 205425.
[49] A. Chaves, F. Peeters, Tunable effective masses of magneto-excitons in two-dimensional materials, Solid State Commun. 334–335 (2021) 114371.
[50] D. Loginov, I. Ignatiev, Giant excitonic magneto-Stark effect in wide GaAs/AlGaAs quantum wells, Phys. E 166 (2025) 116134.
[51] J.M. Luttinger, W. Kohn, Motion of electrons and holes in perturbed periodic fields, Phys. Rev. 97 (4) (1955) 869–883.
[52] R.T. Collins, L. Viña, W.I. Wang, L.L. Chang, L. Esaki, K. v. Klitzing, K. Ploog, Mixing between heavy-hole and light-hole excitons in GaAs/$Al_xGa_{1-x}As$ quantum wells in an electric field, Phys. Rev. B 36 (1987) 1531–1534.
[53] P. Grigoryev, M. Chukeev, V. Lovtcius, Y.P. Efimov, S. Eliseev, Zeeman splitting of excitons in GaAs/AlGaAs quantum wells in the Faraday geometry, J. Exp. Theor. Phys. 137 (5) (2023) 656–663.
[54] E.S. Khramtsov, P.A. Belov, P.S. Grigoryev, I.V. Ignatiev, S.Y. Verbin, S.L. Yakovlev, Theoretical modeling of exciton-light coupling in quantum wells, J. Phys.: Conf. Ser. 690 (2016) 012018.
[55] P.A. Belov, S.L. Yakovlev, Energy levels of excitons in square quantum wells, in: International Conference on Few-Body Problems in Physics, Springer, 2018, pp. 29–33.
[56] P.A. Belov, Linewidths and energy shifts of electron-impurity resonant states in quantum wells with infinite barriers, Phys. Rev. B 105 (15) (2022) 155417.
[57] Y. Shinozuka, M. Matsuura, Wannier exciton in quantum wells, Phys. Rev. B 28 (8) (1983) 4878–4881.
[58] B. Gerlach, J. Wüsthoff, M.O. Dzero, M.A. Smondyrev, Exciton binding energy in a quantum well, Phys. Rev. B 58 (16) (1998) 10568–10577.
[59] P.S. Grigoryev, A.S. Kurdyubov, M.S. Kuznetsova, I.V. Ignatiev, Y.P. Efimov, S.A. Eliseev, V.V. Petrov, V.A. Lovtcius, P.Y. Shapochkin, Excitons in asymmetric quantum wells, Superlattices Microstruct. 97 (2016) 452–462.
[60] R.B. Lehoucq, D.C. Sorensen, C. Yang, ARPACK Users' Guide: Solution of Large-Scale Eigenvalue Problems with Implicitly Restarted Arnoldi Methods, SIAM, 1998.
[61] G. Bastard, Superlattice band structure in the envelope-function approximation, Phys. Rev. B 24 (1981) 5693–5697.
[62] P.A. Belov, E.S. Khramtsov, The binding energy of excitons in narrow quantum wells, J. Phys. Conf. Ser. 816 (2017) 012018.
[63] P.A. Belov, E.S. Khramtsov, P.S. Grigoryev, I.V. Ignatiev, Numerical study of the exciton-light coupling in quantum wells, in: 2017 Progress in Electromagnetics Research Symposium - Spring, PIERS, IEEE, 2017.
[64] S.I. Pokutnyĭ, Excition states in semiconductor quantum dots in the modified effective mass approximation, Semiconductors 41 (11) (2007) 1323–1328.
[65] M. Kumagai, T. Takagahara, Excitonic and nonlinear-optical properties of dielectric quantum-well structures, Phys. Rev. B 40 (18) (1989) 12359–12381.
[66] J.H. Davies, The Physics of Low-dimensional Semiconductors, Cambridge University Press, 1997.
[67] P.A. Belov, Increase in the radiative decay rate of the indirect exciton due to application of the magnetic field, J. Phys.: Conf. Ser. 1851 (1) (2021) 012011.
[68] I. Vurgaftman, J.R. Meyer, L.R. Ram-Mohan, Band parameters for III–V compound semiconductors and their alloys, J. Appl. Phys. 89 (2001) 5815.
[69] L. Landau, E. Lifshitz, Nonrelativistic Quantum Mechanics, Pergamon Press Oxford, 1965.
[70] Because of different masses of electrons and holes, the distribution along the ρ coordinate should be different for different particles. We do not consider here this effect because we are mainly interested in the distribution along the z coordinate.
[71] D.A.B. Miller, D.S. Chemla, T.C. Damen, A.C. Gossard, W. Wiegmann, T.H. Wood, C.A. Burrus, Electric field dependence of optical absorption near the band gap of quantum-well structures, Phys. Rev. B 32 (1985) 1043–1060.
[72] A.S. Kurdyubov, A.V. Trifonov, I.Y. Gerlovin, B.F. Gribakin, P.S. Grigoryev, A.V. Mikhailov, I.V. Ignatiev, Y.P. Efimov, S.A. Eliseev, V.A. Lovtcius, M. Aßmann, M. Bayer, A.V. Kavokin, Optical control of a dark exciton reservoir, Phys. Rev. B 104 (2021) 035414.
[73] B.F. Gribakin, E.S. Khramtsov, A.V. Trifonov, I.V. Ignatiev, Exciton-exciton and exciton–charge carrier interaction and exciton collisional broadening in GaAs/AlGaAs quantum wells, Phys. Rev. B 104 (20) (2021) 205302.
[74] The nonradiative broadening can depend on the applied electric field as it is observed, e.g., in Ref. [24]. However, the exact mechanism of this dependence is unknown.